Fuel 126 (2014) 85–95

Contents lists available at ScienceDirect

Fuel

journal homepage: www.elsevier.com/locate/fuel

# Monitoring the degradation and the corrosion of naphthenic acids by electrospray ionization Fourier transform ion cyclotron resonance mass spectrometry and atomic force microscopy

Heloísa P. Dias [a], Thieres M.C. Pereira [a], Gabriela Vanini [a], Pedro V. Dixini [a], Vinicius G. Celante [b], Eustáquio V.R. Castro [a], Boniek G. Vaz [c,*], Felipe P. Fleming [d], Alexandre O. Gomes [d], Glória M.F.V. Aquije [e], Wanderson Romão [a,e,*]

[a] Petroleomic and Forensic Laboratory, Department of Chemistry, Federal University of Espírito Santo, 29075-910 Vitória, ES, Brazil
[b] Federal Institute of Education, Science and Technology of Espírito Santo, 29192-733 Aracruz, ES, Brazil
[c] Chemistry Institute, Federal University of Goiás, 74001-970 Goiânia, GO, Brazil
[d] Petróleo Brasileiro S/A – PETROBRAS, CENPES, Rio de Janeiro, RJ, Brazil
[e] Federal Institute of Education, Science and Technology of Espírito Santo, 29106-010 Vila Velha, ES, Brazil

## HIGHLIGHTS

- Analysis of naphthenic acids by ESI(-) FT-ICR MS and characterization by AFM of AISI 1020 steel naphthenic corrosion.
- The corrosion text was evaluated in a closed system in reflux at reduced pressure with temperature of 280–350 °C.
- As temperature increases, we observe thermal decarboxylation of naphthenic acids.
- DBE *versus* carbon number shows the trends of the thermal decarboxylation of naphthenic acids.
- AFM measurements evidenced that naphthenic acid corrosion occurred by pitting mechanism.

## ARTICLE INFO

*Article history:*
Received 22 November 2013
Received in revised form 13 February 2014
Accepted 15 February 2014
Available online 28 February 2014

*Keywords:*
Petroleomic
Naphthenic acids corrosion
ESI(-)FT-ICR MS
Atomic force microscopy

## ABSTRACT

Although the term "naphthenic acids" was originally used to describe acids that contain naphthenic rings, today this term is used in a more general sense and refers to all components in the acid extractable fraction. In crude oil, naphthenic acids exist as a complex mixture of compounds with broad polydispersity with respect to both molecular weight and structure. There has been increasing interest in the naphthenic acids in crude oil because of the corrosion problems that cause during oil refining. Herein, two powerful analytical tools, negative-ion electrospray ionization Fourier transform ion cyclotron resonance mass spectrometry, ESI(-)FT-ICR MS and atomic force microscopy (AFM), were combined to monitor the thermal degradation of naphthenic acids and their corrosion effects on AISI 1020 steel, respectively. Two different acidic crude oils (TAN = 2.38 and 4.79 mg KOH $g^{-1}$, and total sulfur = 0.7993 and 1.0220 wt%) have been submitted to thermal treatment at 280, 300 and 350 °C during 2, 4 and 6 h, and characterized by ESI(-)-FT-ICR MS, total acid number (TAN), and total sulfur. The AISI 1020 steel was analyzed by scanning electron microscopy (SEM) and AFM. Generally, heating the crude oil at 350 °C in a period of 6 h, it was observed that a high efficiency (≅80%) and selectivity of thermal decarboxylation process was monitored by decay of TAN (4.79 → 0.44 mg KOH $g^{-1}$). ESI(-)-FT-ICR MS results showed that naphthenic acid species remained after the heating have DBE ranging 1–12 and carbon number from $C_{15}$ to $C_{45}$. AFM topographic profile evidenced that the naphthenic acid corrosion of the crude oil with TAN of 4.73 mg KOH $g^{-1}$ on AISI 1020 steel was profoundly altered and a marked reduction in peak to peak height values (obtained by subtracting the value of the lowest peak by the highest peak in the topographic area examined). Optical images and microphotographs confirmed the presence of irregularities, characterizing the corrosion mechanism as pitting type. The naphthenic corrosion was also evidenced in samples with low TAN value (0.44 mg KOH $g^{-1}$).


* Corresponding authors. Address: Petroleomic and Forensic Laboratory, Department of Chemistry, Federal University of Espírito Santo, 29075-910 Vitória, ES, Brazil. Tel.: +55 27 3149 0833 (W. Romão). Tel.: +55 62 3521 1016 R261 (B.G. Vaz).
*E-mail addresses:* boniek@ufg.br (B.G. Vaz), wandersonromao@gmail.com (W. Romão).

http://dx.doi.org/10.1016/j.fuel.2014.02.031
0016-2361/

## 1. Introduction

Crude oil extraction, transport, and its processing in refineries raise a multitude of challenges for the industry, and can be expressed in economic costs and benefits. Reducing the production costs entices the oil companies to process "opportunity crudes" – low quality corrosive crude oils with high naphthenic acid and sulfur contents that are cheaper than the so called "sweet crudes", the former of which are readily available on the oil market. Processing these acidic crudes at high temperatures in refineries forced the refinery engineers to adopt special strategies for mitigating their corrosive effects. These strategies included blending crudes, selecting better materials for various critical refinery components. Part of the strategy for identifying better materials includes an investment into better understanding the mechanism of naphthenic acid corrosion [1].

Naphthenic acids were identified as the main corrosive species in acidic crudes although they represent less than 3 wt% [2]. They include all organic acids in the acid extractable fraction, but the main constituents are carboxylic acids with general formula R–$(CH_2)_n$–COOH where R corresponds to one or more cyclopentane or cyclohexane rings. Due to naphthenic corrosivity effects and their biological marker role in geochemistry many studies were focused on identification of naphthenic acids structures present in different crudes [3]. This challenge proved to be very difficult because naphthenic acids formed complicated mixtures. Some references mentioned that only in a single crude oil sample contains approximately 1500 different organic acids identified with molecular weights ranging from 200 to 700 Da. [1,4]. More recent works on some crude oils identified naphthenic over a mass range of 115–1500 Da with a carbon content of $C_{20}$–$C_{80}$ [4].

Measuring naphthenic acids concentration in oils was one of the first tasks for naphthenic corrosion studies. Currently, naphthenic concentrations are measured by titrating them with an alcoholic solution of potassium hydroxide (KOH), being expressed by the total acid number (TAN) that represents the milligrams of KOH used to neutralize all acidic species in 1 g of oil sample [5]. Crude oils with TAN > 0.5 mg of KOH $g^{-1}$ may cause severe corrosion problems to refining operations [6–8]. However, the TAN is not directly correlated with the corrosivity of naphthenic acids. It depends upon the size and structure of the naphthenic acids [4] present and the interaction of naphthenic acids with other compounds present in the crude oil (sulfites, carbon dioxide, etc.).

Fourier transform ion cyclotron resonance mass spectrometry (FT-ICR MS) offers the highest available mass resolution, mass resolving power, and mass accuracy, which enable the analysis of complex petroleum mixtures on a molecular level [9]. High-resolution MS data have shown that it is possible to discriminate different compounds [10–12] because of the different ionization efficiencies of the crude oil constituents [13]. Accurate mass measurements [14,15] allow unambiguous elemental composition ($C_cH_hN_nO_oS_s$) assignment and double bond equivalent (DBE), facilitating material classification by heteroatom content and the degree of aromaticity [16–18]. Naphthenic acids can be analyzed by negative-ion electrospray ionization, ESI(-), coupled to FT-ICR MS, being detected in form of deprotonated molecule, $[M–H]^-$ [19,20].

Some studies in literature report the correlation between the chemical composition of crude oil and the corrosion process [21–23]. In 2012, Huang et al. [21] studied the synergy effect of naphthenic acid corrosion and sulfur corrosion at high temperature (280 °C) in a crude oil distillation unit using Q235 carbon–manganese steel and 316 stainless steel. In a corrosion media containing only sulfur (from 1 to 5 wt%), the corrosion rate of Q235 and 316 first increased and then decreased with the increasing of sulfur content. However, when the naphthenic acid and the sulfur compounds were added together a synergy effect on the corrosion rate was observed in Q235 and 316. In the same year, Freitas et al. [22] studied the effect of composition of heavy distillation cuts from heavy crude oil (density = 0.93 and TAN = 1.93 mg KOH $g^{-1}$) on the corrosion process. The cuts with boiling temperatures lower than 315 °C and TANs ranging from 0.47 to 1.83 mg $g^{-1}$ were studied. According to the ESI(-)-FT-ICR MS results, the naphthenic acid species were detected in the six cuts studied (cuts 2–7), with $m/z < 300$ and DBEs ranging from 2 to 4. Similarly, the relative abundance of heavy naphthenic acids and the TAN increase with the distillation cut temperature. This information correlated with the corrosion mechanism for AISI 1020 steel in the heavy oil and the distillation cuts, where the corrosion was more evident in the oil distillation cuts that were characterized as alveolar and pitting. In addition, Piehl [24] and Slavcheva et al. [7] show that the corrosion rate had increased (from 0.30 mm $y^{-1}$ to 1.27 mm $y^{-1}$) as a function of boiling point (from 204 °C to 371 °C) for cuts with TAN ≅ 2 mg KOH $g^{-1}$. It also increased (from 1.27 mm/y to 2.08 mm/y) as a function of TAN (from 2 mg KOH $g^{-1}$ to 10 mg KOH $g^{-1}$) at 371 °C [25]. In 2013, our group shows that heavy distillation cuts are more corrosive than the light distillation cuts, where the corrosion rate will increase in the following order: naphtha (cuts 1-2) < kerosene (cuts 3-4) < gas oil (cuts 5-12), being the corrosion process caused by both: naphthenic acids and sulfur compound species [18], which are primarily present in the heavy distillation cuts.

Recently, alternative methods have been developed to reduce the amount of naphthenic acid species and consequently the corrosion rate [26–28]. These processes normally involve critical and expensive conditions such as high temperatures (300–400 °C) and an inert $N_2$ atmosphere [22], the use of supercritical water in a batch reactor at 500 °C and 50 MPa [23] or thermal cracking and catalytic decarboxylation over alkaline earth-metal oxides and ZnO catalysts [24]. Herein, two different acidic crude oils (TAN = 2.38 and 4.79 mg KOH $g^{-1}$, and total sulfur = 0.7993 and 1.0220 wt%) were submitted to thermal treatment at 280, 300 and 350 °C during 2, 4 and 6 h, being then monitored by ESI(-)-FT-ICR MS, TAN, total sulfur, and scanning electron (SEM) and atomic force (AFM) microscopies. The correlation between the chemical composition and the corrosion was analyzed.

## 2. Experimental

### 2.1. Materials and reagents

Anhydrous propan-2-ol, toluene and potassium hydroxide (KOH, analytical grades with purity higher than 99.5%) were used for the TAN measurements. Acetone and kerosene were used in washing of the 1020 steel, applied in corrosion experiments. These chemicals were supplied by Vetec Química Fina Ltda, Brazil. Ammonium hydroxide ($NH_4OH$) and sodium trifluoroacetate (NaTFA) purchased from Sigma–Aldrich Chemicals USA and used for the ESI(-)-FT-ICR MS measurements. All reagents were used as received.

### 2.2. Primary characterization of the crude oils

Two samples of offshore oils from Espírito Santo state (ES), Brazil, were characterized according to the standards of the American Society for Testing and Materials (ASTM) by Laboratory of Petroleum Characterization of Federal University of Espírito Santo (LabPetro/UFES-Brazil). A primary characterization was conducted to determine the total acid number (ASTM D664-09) [4,29], and the total sulfur (ASTM D4294) analyses. [26,30] The data obtained from the

characterization of two crude oils termed in A and B are as follows: TAN = 2.38 and 4.79 mg KOH $g^{-1}$, and total sulfur = 0.7993 and 1.0220 wt%, respectively (see Table 1).

### 2.3. Thermal degradation of crude oils

A homemade distillation process (accordance with ASTM D 2892) [31] was used to study the naphthenic acids thermal degradation. Initially, distillation system was loaded with approximately 400 mL of crude oil and heated from 20 °C to three final aging temperatures: 280, 300 and 350 °C. The time ageing was varied from 2 to 6 h under a closed system in reflux at reduced pressure from 760 to 0.1 mm Hg. Fig. 1 summarizes an experimental scheme developed to study the thermal degradation of naphthenic acids from two acidic crude oils (A and B). Aged oils were produced and termed in $A_m$ and $B_n$ where $m$ = 1–6 and $n$ = 1–9, Fig. 1 and Table 1. After, all samples (original and aged) were characterized in terms of TAN, total sulfur and ESI(-)-FT-ICR MS. The total sulfur and the TAN values are shown in Table 1.

### 2.4. ESI(±)-FT-ICR MS

Petroleum samples were analyzed by both ion modes: positive and negative electrospray ionization, ESI(±). Briefly, the samples were diluted to ≈1 mg $mL^{-1}$ in 50:50 (v/v) toluene/methanol which contained 0.1% *m/v* of $NH_4OH$ for ESI(-) and 0.1% *m/v* of HCOOH for ESI(+). The resulting solution was directly infused at a flow rate of 4 μl $min^{-1}$ into the ESI source. The mass spectrometer (model 9.4 T Solarix, Bruker Daltonics, Bremen, Germany) [17,18,26,32] was set to operate over a mass range of *m/z* 200–1300. The ESI(-) source conditions were as follows: a nebulizer gas pressure of 3 bar, a capillary voltage of 3 kV, and a transfer capillary temperature of 250 °C. The ion accumulation time in the hexapole was 0.02–0.03 s, followed by transport to the analyzer cell (ICR) through the multipole ion guide system (another hexapole). Each spectrum was acquired by accumulating 200 scans of time-domain transient signals in 4 mega-point time-domain data sets. The front and back trapping voltages in the ICR cell were −0.60 V and −0.65 V for ESI(-) and +0.80 V and +0.85 V for ESI(+), respectively. All mass spectra were externally calibrated using a NaTFA solution (*m/z* from 200 to 1200) after they were internally recalibrated using a set of the most abundant homologous alkylated compounds for each sample [18]. A resolving power, $m/\Delta m_{50\%} \cong 460{,}000–500{,}000$, in which $\Delta m_{50\%}$ is the full peak width at half-maximum peak height, of *m/z* 400 and a mass accuracy of <1 ppm provided the unambiguous molecular formula assignments for singly charged molecular ions. The mass spectra were acquired and processed using a custom algorithm developed specifically for petroleum data processing, Composer software (Sierra Analytics, Pasadena, CA, USA). The MS data were processed, and the elemental compositions of the compounds were determined by measuring the *m/z* values. To help visualize and interpret the MS data, typical plots such as DBE *versus* carbon number and heteroatomic-containing compounds profile were constructed.

### 2.5. Scanning electron and atomic force microscopies analyses

Atomic force microscopy (AFM), invented in 1986, is a powerful imaging technique for nanoscale investigation [33], permitting highly sophisticated surface morphology characterization. It is based on imaging (visualization) of the surface of a sample with high resolution at nanoscale dimensions [34,35]. The basic idea

**Table 1**
Physical–chemical characterization of crude oils A and B, and their thermal degradation products.

| Temperature | Time (h) | TAN (mg KOH $g^{-1}$) | | Sulfur (wt%) | |
|---|---|---|---|---|---|
| | | Sample A | Sample B | Sample A | Sample B |
| 280 | – | 2.38 (A) | 4.79 (B) | 0.7993 (A) | 1.0220 (B) |
| | 2 | 3.39 ($A_1$) | 5.00 ($B_1$) | 0.6080 ($A_1$) | 0.9846 ($B_1$) |
| | 4 | 3.27 ($A_2$) | 5.05 ($B_2$) | 0.6079 ($A_2$) | 0.9879 ($B_2$) |
| | 6 | 3.18 ($A_3$) | 4.74 ($B_3$) | 0.6089 ($A_3$) | 1.0134 ($B_3$) |
| 300 | 2 | 2.66 ($A_4$) | 4.73 ($B_4$) | 0.5880 ($A_4$) | 1.0102 ($B_4$) |
| | 4 | 1.90 ($A_5$) | 4.59 ($B_5$) | 0.5729 ($A_5$) | 1.0052 ($B_5$) |
| | 6 | 1.95 ($A_6$) | 4.06 ($B_6$) | 0.6028 ($A_6$) | 1.0081 ($B_6$) |
| 350 | 2 | – | 3.35 ($B_7$) | – | 0.9436 ($B_7$) |
| | 4 | – | 4.23 ($B_8$) | – | 0.9770 ($B_8$) |
| | 6 | – | 0.44 ($B_9$) | – | 0.9580 ($B_9$) |

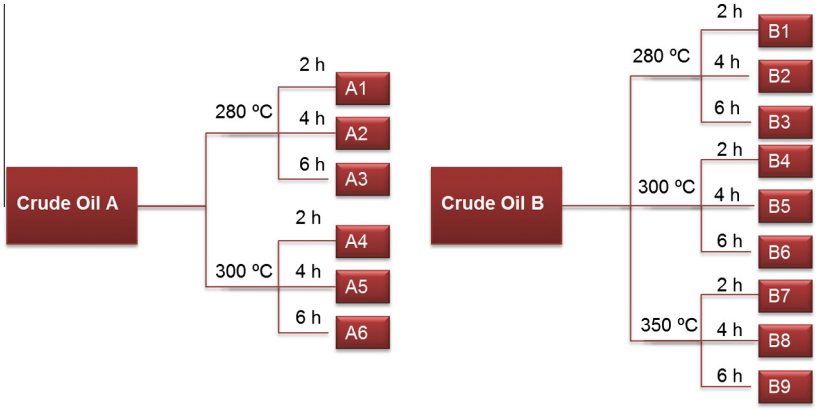


**Fig. 1.** Scheme of thermal degradation for two crude oils samples (A and B) submitted to heating temperature of 280, 300 and 350 °C during 2, 4 and 6 h, respectively.

behind AFM is to scan a sharp tip over the surface of a sample, becoming possible to measure the interaction force between the tip and the sample. This allows three-dimensional images to be generated, being mounted on a piezoelectric scanner [36]. Here, scanning electron microscopy (SEM) and AFM analyses were realized, *in situ*, on 1020 steel without (blank) and exposed to the corrosive effects caused by two crude oils samples aged with varied degrees of acidity: $B_4$ and $B_9$ with TANs of 4.73 and 0.44 mg KOH $g^{-1}$, respectively.

To characterize the type of corrosion present in AISI 1020 steel, samples were washed with acetone, polished with 120- to 1220-grit sandpaper, and immersed in a bath with acetone under ultrasonication for 10 min. The AISI 1020 steel samples were then immersed in containers of 10 mL with aged samples B4 and B9. After a period of 15 days (or 360 h), the specimens were washed with acetone and kerosene. Immediately after drying, SEM/Energy Dispersive Spectroscopy (EDS) and AFM images were taken in a Shimadzu SSX 500 (Kyoto, Japan) without metallization operating at 12 kV and an Alpha 300R confocal microscope (WITEc/Wissenschaftliche Instrumente und Technologie GmbH®, Ulm, Germany), respectively. For AFM measurements, the topographic images were made in non-contact mode (from regions selected by use of the integral light microscope), with $Si_3N_4$ cantilever tips, nominal constant of 42 N $m^{-1}$; resonance frequency of ≈285 kHz, scan rates of 0.3–1.0 Hz and scan size of 2500–10,000 nm. Peak to peak height parameter (obtained from cross section of topography image) was monitored and used to evaluate the surface roughness morphology.

## 3. Results

The physical–chemical characterization (total sulfur and TAN) of crude oils (A and B) and their degradation products ($A_m$ and $B_n$ where $m$ = 1–6 and $n$ = 1–9) are shown in Table 1. For the original oils A and B, TAN and the total sulfur (or S content) values are of 2.38 and 4.79 mg KOH $g^{-1}$; 0.7993 and 1.0220 wt%, respectively, being expected that the sample B have a higher corrosivity. When crude oil A was submitted to thermal degradation, a reduction of 20% and 25% of TAN (2.38 → 1.95 mg KOH $g^{-1}$) and S content (0.7993 → 0.6028 wt%), respectively, was observed at 300 °C and 6 h of aging (sample $A_6$), Table 1. The reproducibility of thermal decarboxylation of naphthenic acids was confirmed by reduction of TAN in 16%, when another crude oil, sample B, was submitted to same thermal degradation conditions (300 °C and 6 h of aging time, $TAN_B$ = 4.79 mg KOH $g^{-1}$ → $TAN_{B6}$ = 4.06 mg KOH $g^{-1}$). Sulfur heteroatom compound species undergo a little reduction, 1.0220 wt% ($S_B$) → 1.0081 wt% ($S_{B6}$), Table 1.

With of aim of improving the efficiency and selectivity of thermal decarboxylation method, the heating temperatures were increased (300 → 350 °C) and a reduction higher than 80% was obtained for sample $B_9$. In contrast to naphthenic acids species, sulfur heteroatom compound species remains stable within of oil (reduction of only 7%), thus proving, their higher thermal stability [18]. Naphthenic acid species can experience thermal-degradation reactions and produce low chain length naphthenic acids ($C_1$–$C_4$), which are favored by its low aromaticity [17,26] or can also

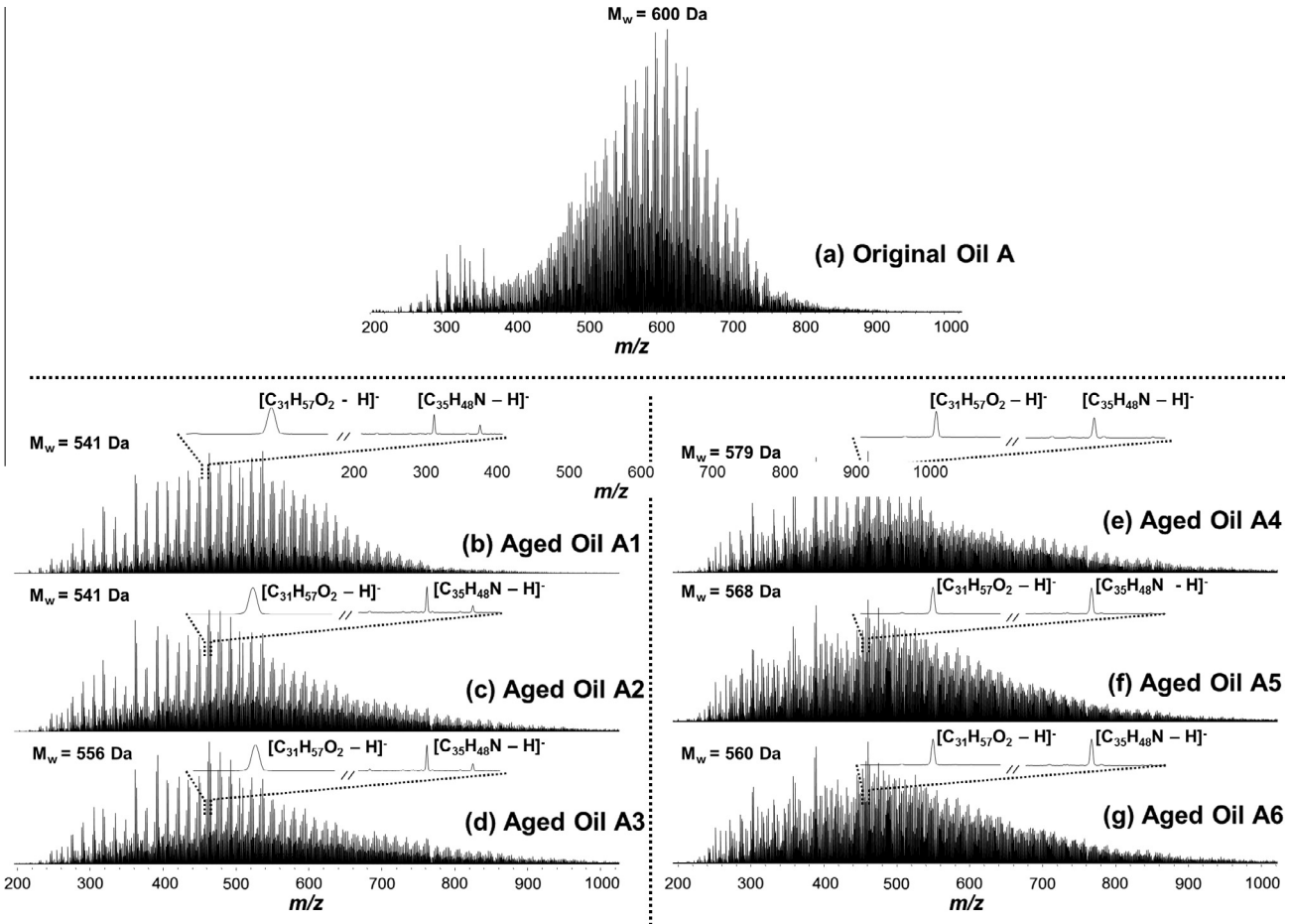


**Fig. 2.** ESI(-)-FT-ICR MS for the crude oil A (a) and yours degradation products submitted at heating temperature of 280 °C (during 2 (b), 4 (c) and 6 h (d)) and 300 °C (during 2 (e), 4 (f) and 6 h (g)). The insert shows that the intensity of ion $[C_{31}H_{57}O_2–H]^-$ of *m/z* 459.4207 and DBE of 4 decreases whereas the ion $[C_{35}H_{48}N–H]^-$, of *m/z* 480.3636 and DBE of 13, increases in function of heating temperature and aging time.

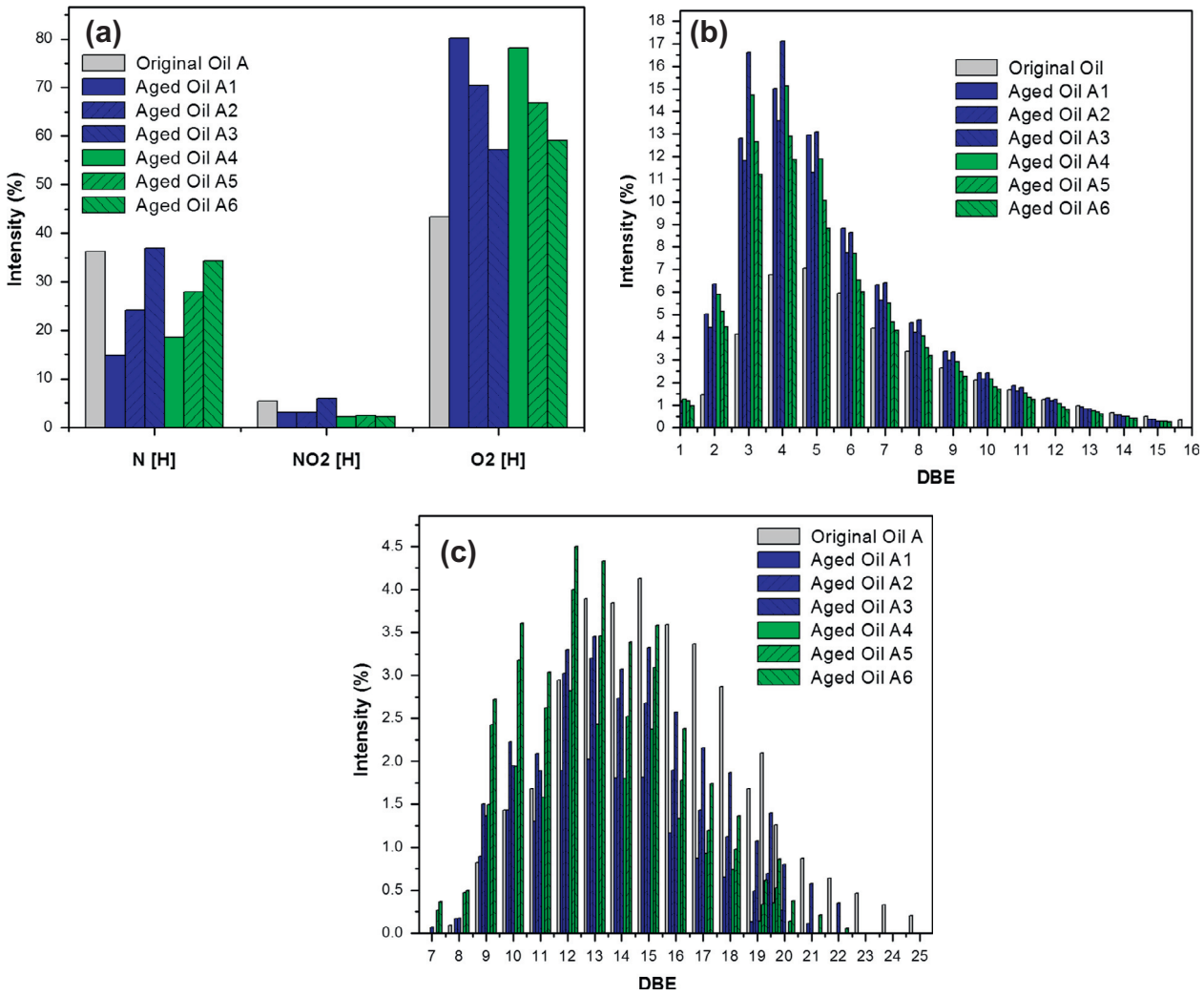


**Fig. 3.** (a) Heteroatom-containing compound class distribution; and relative abundances for O2 (b) and N (c) compound classes from ESI(-)-FT-ICR MS data of crude oil A and yours degradation products at 280 and 300 °C during 2, 4 and 6 h. Maxima abundance of DBEs of 5 and 15 is observed for naphthenic acids and carbazoles species, respectively. These values decrease (DBE = 3–4 and 12–15 for O2 and N classes, respectively) after thermal degradation is performed.

undergo decarboxylation reactions as a consequence of these poor thermal stability [28,37].

Non-typical behavior was observed for both crude oils when were submitted to heating temperature of 280 °C (temperature lower than thermal cracking conditions), Table 1. For degraded crude oils $A_1$, $A_2$, $A_3$, $B_1$ and $B_2$, an increasing in TAN is observed in relation to original crude oil. It is due to oxidation and hydrolysis reactions or disaggregation of heavy fractions presents in crude oil such as asphalthenes [24,38,39].

### 3.1. ESI(-)-FT-ICR MS

Fig. 2 shows the ESI(-)-FT-ICR mass spectra for original crude oil A (2a) and its degradation products submitted at heating temperature of 280 °C ($A_1$, $A_2$ and $A_3$, 2b–d) and 300 °C ($A_4$, $A_5$ and $A_6$, 2e–g). In general, the ESI(-)-FT-ICR mass spectra have profiles from *m/z* 200 to 1000 with an average molar mass distribution ($M_w$) centered from ≅600 Da (for original oil A, Fig. 2a) to 540–580 Da (for aged oils, Fig. 2b–g). Heteroatom-containing species were detected as deprotonated molecules, that is, $[M–H]^-$ ions, corresponding primarily to naphthenic acids and carbazole analog species.

As a consequence of the removal of naphthenic acid species from crude oil, a decrease in $M_w$ was observed in the mass spectra for the aged oils (Fig. 2b–g). The enlarged area around *m/z* 459 and 480 (Fig. 2b–g) highlights the slight decrease in the intensity of the $[C_{31}H_{57}O_2–H]^-$ ion, which has an *m/z* of 459.4207 and DBE of 4; whereas the $[C_{35}H_{48}N–H]^-$ ion, of *m/z* 480.3636 and DBE of 13, increases in function of heating temperature and time.

Generally, petroleum samples have chemical compositions that differ significantly from one another. One way to display the similarities or differences between the signal patterns of crude oil samples is to construct certain types of plots, such as plots of the relative abundances of different classes of compounds and of the DBE *versus* the carbon number [26].

In the present study, for the class profile diagrams, Fig. 3a, the relative amounts of each class were calculated by summing abundances in one compound class and dividing by the total abundance of all species. The relative amounts of N, $NO_2$ and $O_2$ compounds present in the crude oil A and your degradation products are presented in Fig. 3a. In all cases, the $O_2$ class, composed primarily of naphthenic acids, was the most abundant class. The N class (pyrrolic analog species) was the second most abundant, followed by the $NO_2$ class (analogous to pyrrolic or pyridines with one carboxylic acid group or two hydroxylic groups). Initially, it should be noted that the relative abundance of $O_2$ compounds increased at 280 °C and 2 h (∼44 → ∼80%), after decreasing simultaneously in function

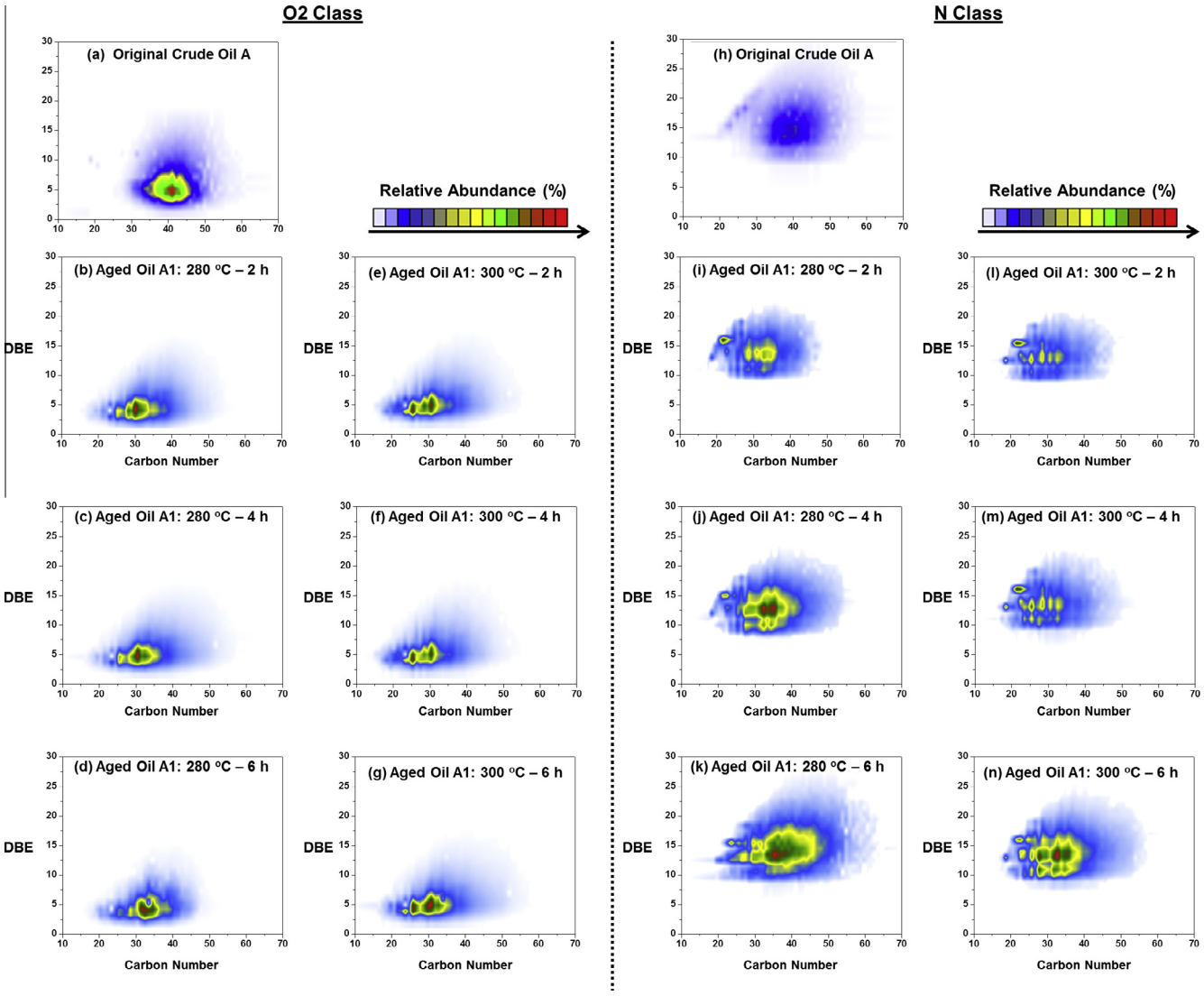


**Fig. 4.** Plot of DBE *versus* carbon number for $O_2$ and N classes of crude oil A (a, h) and your degradation products (b–g for O2 class; and i–n for N class). The carbon number abundance distribution maximum decreased from ≈$C_{42}$ (crude oil, 4a) to ≈$C_{30}$ (aged oils, 4b–g) for O2 class. Similar behavior is also observed for carbazoles species (N class), having your carbon number raging from $C_{20}$–$C_{60}$ (4 h) to $C_{16}$–$C_{53}$ (4i–n).

of heating temperature (~80% (280 °C) → ~76% (300 °C) during the period of 2 h) and of heating time (~80% (2 h) → ~58 (6 h)%), Fig. 3a.

Fig. 3b and c shows the relative abundance distributions for the $O_2$ (3b) and N (3c) compound classes in crude oil A and its degradation products. For original oil A, naphthenic acids and carbazoles species with DBEs of 4–7 and 14–16 are majority presents, respectively, Fig. 3b and c. As consequence of thermal degradation process, these values are reduced to DBEs of 3–5 (for $O_2$ class, 3b) and 12–15 (for N class, 3c).

Plots of the DBE *versus* the carbon numbers have proven to be useful tools for the differentiation of complex organic mixtures based on chemical composition. It has been shown that these plots allow the presentation of all signals from a specific class in a simple and feasible way [40,41]. For this reason, to qualitatively compare the crude oil A and its degradation products, DBE *versus* carbon number plots were generated, showing the distribution of all components from a specific class. Each horizontal line of the diagram represents a homologous series with a specific DBE value.

Fig. 4a–n shows plots of the DBE *versus* the carbon number for the O2 and N classes of crude oil A (a, h) and their degradation products (b–g and i–n). For the O2 class, there are compounds with DBEs ranging from 1 to 17 and carbon numbers ranging from $C_{25}$ to $C_{60}$, with the most abundant compounds being $C_{42}$ with a DBE of 4, Fig. 4a. The most abundant $O_2$ compounds were mainly composed of three naphthenic rings, in agreement with the results reported by Schaub et al. [42] and Colati et al. [29]. A notable difference was observed when compare the O2 class from original oil A (Fig. 4a) to your degradation products, Fig. 4b–g. For this class, the amplitude of DBE and carbon distributions decrease as a function of heating time at 280 °C (Fig. 4b–d) and 300 °C (Fig. 4e–g). Initially, the sample $A_1$ contained a series of compounds with DBEs ranging from 1 to 15 (Fig. 4b), including compounds with a wider carbon number distribution (from $C_{15}$ to $C_{55}$). After, for sample $A_3$ (Fig. 4d), a short DBE distribution and carbon number were observed, corresponding to compounds with carbon numbers from $C_{20}$ to $C_{45}$ and DBEs from 1 to 12. Similar behavior is observed among the samples $A_4$, $A_5$ and $A_6$.

Fig. 4h shows the distribution of N compounds for crude oil A. Generally, the range of DBEs was notably higher and wider for the original oil than your degradation products (Fig. 4i–n), with DBEs ranging from 10 to 27 and carbon numbers ranging from

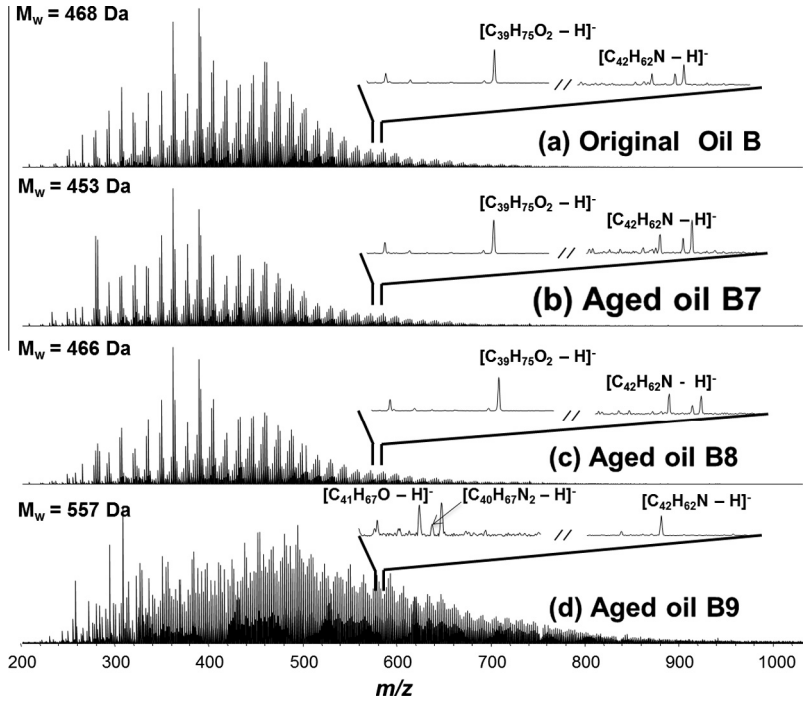


**Fig. 5.** ESI(-)-FT-ICR MS for the crude oil B (a) and yours degradation products submitted at heating temperature of 350 °C (during 2 (b), 4 (c) and 6 (d). The insert shows that the intensity of ion $[C_{39}H_{75}O_2–H]^-$ of *m/z* 573.5612 decreases whereas the ion $[C_{42}H_{62}N–H]^-$ of *m/z* 578.4732 increases in function of aging time; other ions ($[C_{41}H_{67}O–H]^-$ and $[C_{40}H_{67}N_2–H]^-$ with *m/z* 573.5041 and 573.5152, respectively) are only detected in final thermal degradation process, being a indicative of high efficiency in decarboxylation reaction at 350 °C after of a period of 6 h.

$C_{20}$ to $C_{60}$, Fig. 4h. Your degradation products present lower DBEs and carbon numbers values ranging from 7 to 27 and from $C_{16}$ to $C_{53}$, Fig. 4i–n.

Fig. 5 shows the ESI(-)-FT-ICR mass spectra for another original oil, oil B (5a) with TAN of 4.79 mg KOH $g^{-1}$, that was now submitted at higher heating temperature (350 °C during 2, 4 and 6 h, producing the samples $B_7$, $B_8$ and $B_9$, 5b–d). In general, the ESI(-)-FT-ICR mass spectra have similar $M_w$ (~450–470 Da) for samples B, $B_7$ and $B_8$, Fig. 5a–c. A distinct $M_w$ (557 Da) and chemical profile is observed for sample $B_9$, Fig. 5d. The insert shows that the intensity of $[C_{39}H_{75}O_2–H]^-$ ion of *m/z* 573.5612 decreases in function of aging time and disappearing after of a period of 6 h. Consequently, other chemical species are selectively ionized as the $[C_{42}H_{62}N–H]^-$ ion of *m/z* 578.4732 which its relative intensity increases in function of aging time. Additionally, new ions as $[C_{41}H_{67}O–H]^-$ and $[C_{40}H_{67}N_2–H]^-$ of *m/z* 573.5041 and 573.5152 are detected in final thermal degradation process, Fig. 5d. DBE *versus* the carbon number plots for the new compounds classes identified in sample $B_9$ (O, $N_2$, NO and $NO_2$ classes) are shown in Fig. 1S (supplementary material). Therefore, this behavior is a direct indicative of that the thermal decarboxylation process was efficient and selective at 350 °C after of a period of 6 h. This results is good agreeing with TAN data (0.44 mg KOH $g^{-1}$), Table 1.

Fig. 6a–j shows plots of the DBE *versus* the carbon number for the $O_2$ class of crude oil B (a) and its aged oils (b–j) at heating temperature of 280 (b–d), 300 (e–g) and 350 °C (h–j). For the original oil B, there are compounds with DBEs ranging from 1 to 15 and carbon numbers ranging from $C_{15}$ to $C_{50}$, with the most abundant compounds being $C_{26}$ with a DBE of 4, Fig. 6a.

In 2013, Colati et al. [29] developed a liquid/liquid extraction method for two crude oil samples (TAN = 4.95 and 3.19 mg KOH $g^{-1}$) at three different pHs (pH 7, 10 and 14). A decreasing TAN in the original oil was observed with increasing pH (7 → 14), reaching a value of almost zero at pH 14, where naphthenic acids with short alkyl chain lengths (<$C_{44}$) and DBE = 3–4 are primarily responsible for the TAN observed for the original oil. Herein, among two original oils analyzed, the oil B is primarily more acid than oil A ($TAN_A$ = 2.38 mg KOH $g^{-1}$; and $TAN_B$ = 4.79 mg KOH $g^{-1}$), where the presence majority of naphthenic acids with short alkyl chain lengths (≅$C_{26}$) and DBE = 4 is predominantly evidenced for sample oil B.

When compare the plots of DBE *versus* number carbon among aged oils samples $B_{1-9}$, a reduction of amplitude of DBE values (from 1–15 to 1–12) is mainly observed in function of heating time (2 → 6 h) at 280 (Fig. 6b–d), 300 (Fig. 6e–g) and 350 °C (Fig. 6h–j). Finally, despite thermal decarboxylation process show high efficient content and selective at 350 °C after of a period of 6 h, sample B9, Fig. 6j, naphthenic acid species remain presents in oil over a wide amplitude of DBE (1–12) distribution and of carbon number ($C_{15}$–$C_{45}$).

In 2009, Smith et al. [26] have examined suspected molecular transformations of thermally treated Athabasca bitumen heavy vacuum gas oil (HVGO) by ESI(-)-FT ICR MS under an inert $N_2$ atmosphere at temperatures of 300, 325, 350, and 400 °C during a period of 1 h. Basically, the TAN of the HVGO liquid products decreased with an increasing treatment temperature (from 4.13 at 300 °C to 1.46 at 400 °C), indicating a potential carboxylic acid decomposition. ESI(-)FT-ICR MS reveled no compositional changes in the naphthenic acid ($O_2$ class) composition of liquid products. More recently, BaiBing et al. [43] in 2013 have undergone a thermal reaction of Liaohe crude oil at 300–500 °C with a final temperature of 1 h. The $O_2$ class which mainly corresponds to naphthenic acids decarboxylated at 350–400 °C, resulting in a sharp decrease in TAN. The O2 class species in 300 °C and 350 °C reaction products were mostly 1–3 ring naphthenic acids. Similar to our work, they also noticed that the dominant acids in the products were decomposed from large acid species. The compound $C_{18}H_{36}O_2$ (DBE = 1) corresponding to stearic acid, which is related to the most contaminant found in mass spectrometry measurements. Therefore, it is shown here that a long thermal degradation period (time > 4 h) is

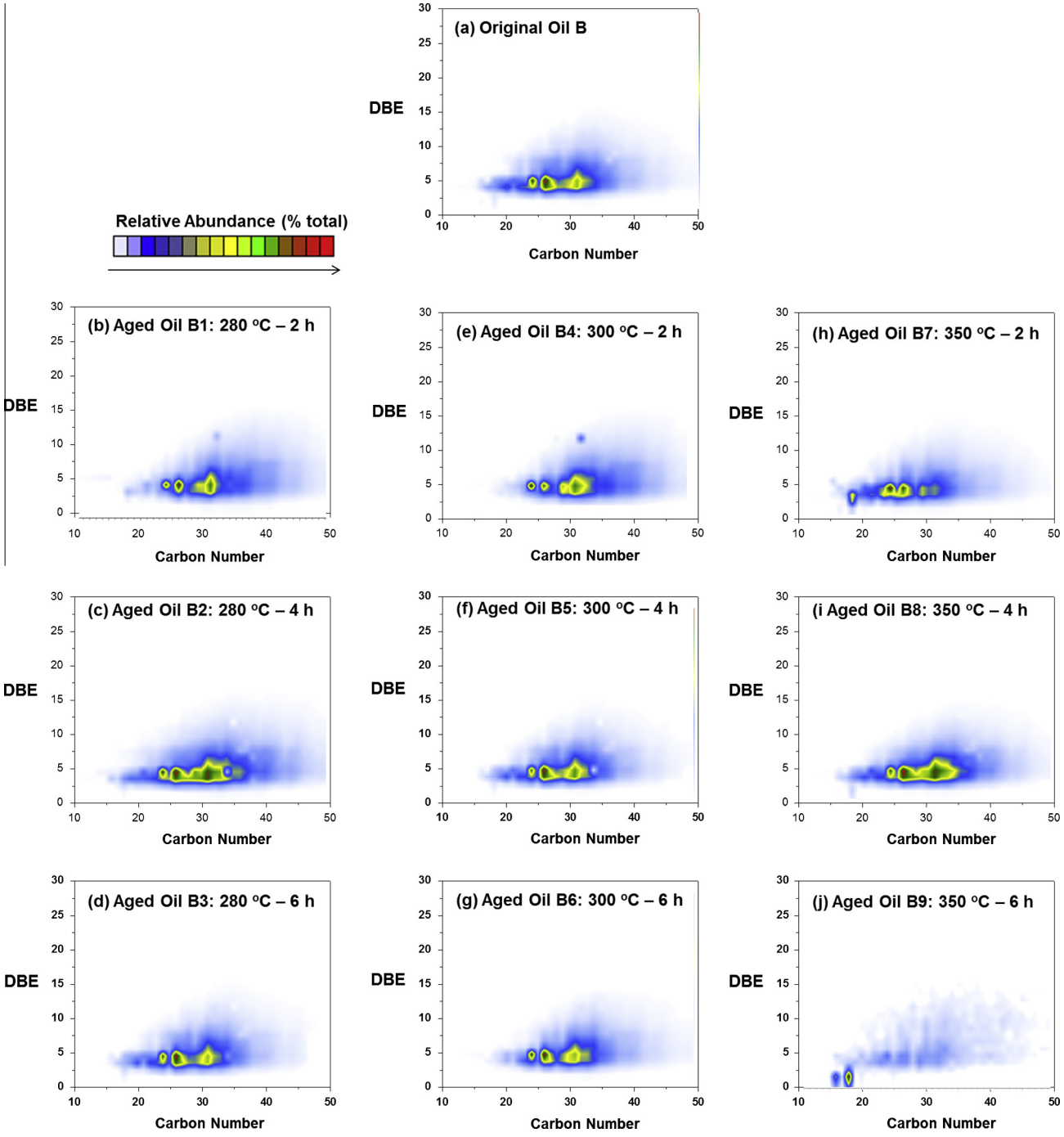


**Fig. 6.** Plot of DBE *versus* carbon number for $O_2$ class of crude oil B (a) and its products thermally degraded at 280 ($B_1$, $B_2$, $B_3$, 6b–d), 300 (B4, B5 and B6, 6e–g) and 350 °C (B7, B8 and B9, 6 h–j).

also crucial for a higher efficiency in the TAN reduction, and consequently, of naphthenic acid species.

Basic nitrogen-containing compound classes (from pyridines derivatives, $N_x$ classes) were analyzed using now ESI(+)-FT-ICR MS data. In general, the ESI(+)-FT-ICR mass spectra for degradation products of crude oil B (samples $B_1$–$B_9$, Fig. 2S) have similar $M_w$ (~505–534 Da, Fig. 2S) and amplitude of distribution of DBE *versus* the carbon number for N (Fig. 3S) and N2 (Fig. 4S) classes, thus proving that the basic nitrogen species have a higher thermal stability than naphthenic acids.

### 3.2. AFM and SEM/EDS

With the aim to evaluate the effect of naphthenic acid corrosion on the AISI 1020 carbon steel surface, two different aged oils of TAN = 0.44 mg KOH $g^{-1}$ (sample $B_4$) and 4.73 mg KOH $g^{-1}$ (sample $B_9$) were selected and their corrosivity studied. Fig. 7 shows images produced from light microscope and AFM analyzes for surface of AISI 1020 steel without crude oil (blank, Fig. 7a, d and g) and after exposure to aged oils $B_9$ (7b, 7e and 7h) and $B_4$ (7c, 7f and 7i) for a period of 15 days. Fig. 7d–f shows images and topographic

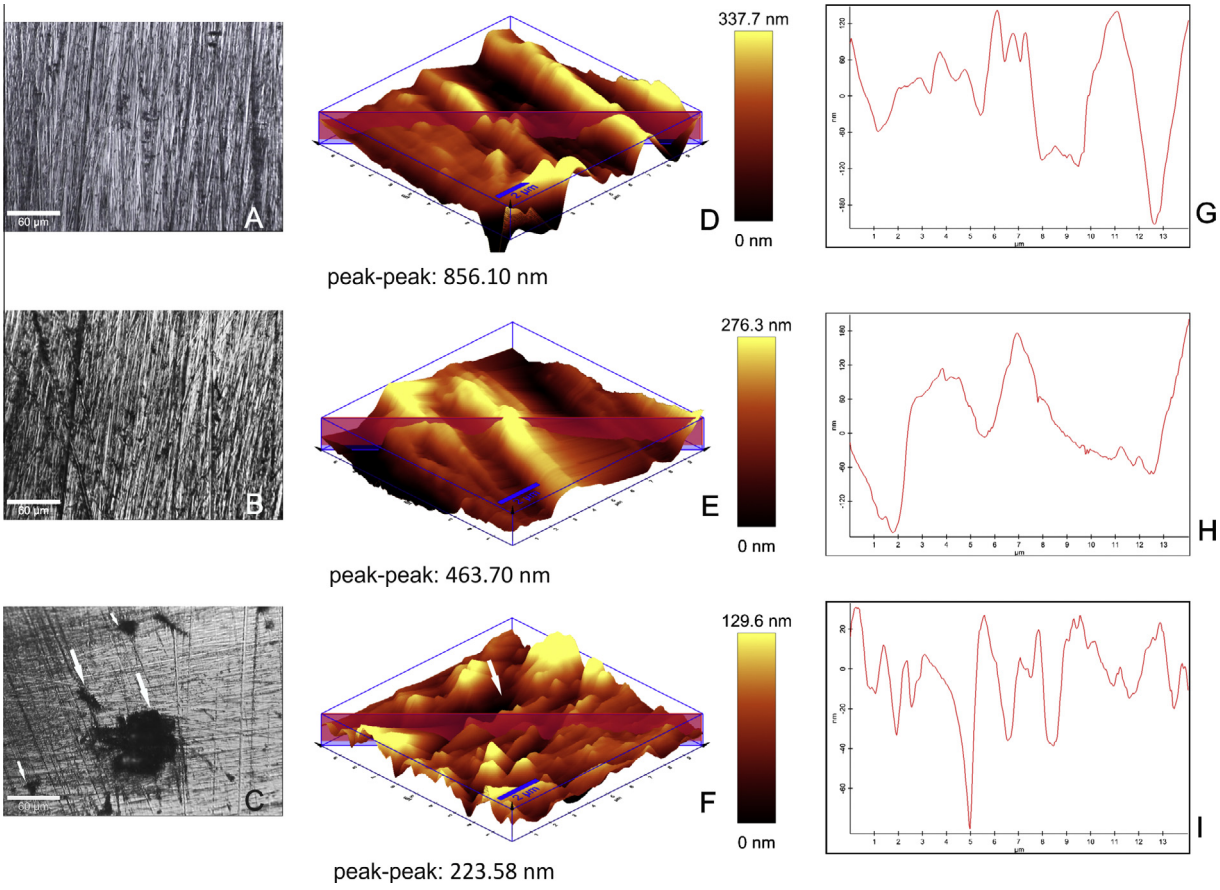


**Fig. 7.** Images produced from light microscopy and AFM analyzes for surface of stainless AISI 1020 without exposure (A, D and G) to petroleum, and after exposure to aged crude oil B9 (B, E and H) and B4 (C, F and I) for a period of 15 days. Figures D, E and F show images and topographic peak–peak height, where the cross section information is detailed from Figures G, H and I. Images produced from AISI exposure to acidic crude oil (B4 with TAN of 4.73 mg KOH $g^{-1}$), evidences the corrosion by pit formation on the steel surface (Figure C, being indicate by a white arrow), producing topographic profile profoundly altered by the formation of peaks on the surface and a marked reduction in peak to peak height values (Figures F and I).

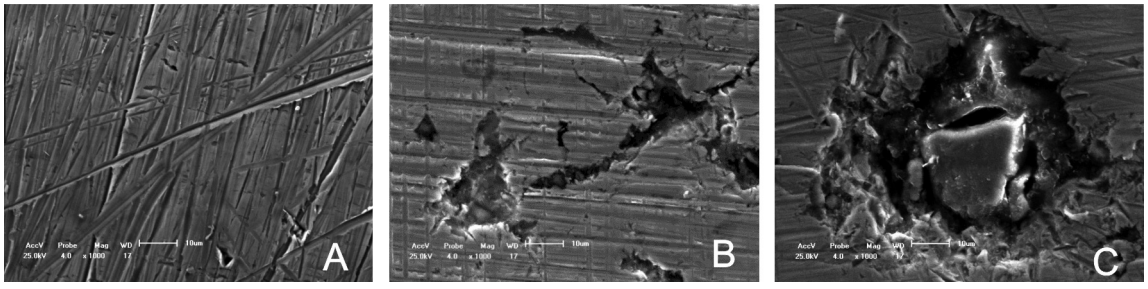


**Fig. 8.** Microphotographs of AISI 1020 steel obtained from SEM analyzes without (A) and with exposure to crude oils B9 (B) and B4 (C). Note the presence of irregularities in steel surface in all cases: in first is due to pre-treating from sanding; whereas that the second and third correspond to alveolar type corrosion, being more severe for AISI 1020/crude oil B4 system.

peak–peak height, where the cross section information is detailed from Fig. 7g–i. For AISI 1020 steel (blank), same irregularities are observed on its surface and can be attributed to pretreatment with grit sandpapers (groove caused by mechanical polishing, Fig. 7a). These irregularities produce topographic profile (from AFM cross section graph, Fig. 7d) with high value of peak-to-peak height (856 nm)[1], reflecting in topographic heterogeneity of the steel's surface and offers an important means of quantifying the roughness of steel [31]. Therefore, peak-to-peak height is an important parameter to monitor *in situ* the corrosion degree on the AISI steel.

When the AISI steel is exposure to low ($B_9$) and high ($B_4$) acidic oils during 15 days, the corrosion is strongly evidenced for $B_4$ sample by the appearance of an eroded area on the surface. These erosions have a larger diameter and then its depth indicates an alveolar corrosion type, on the steel surface, being the eroded area indicated in Fig. 7c by a white arrow [16]. Consequently, the topographic profile (observed from cross section graph, Fig. 7f) was profoundly altered by the formation of peaks on the surface and a marked reduction in peak to peak height values (from 856 to

[1] Peak–peak height is obtained by subtracting the value of the lowest peak by the highest peak in the specific area examined.

**Table 2**
Qualitative data from microanalysis by EDS.

| Samples | Micro analysis by Energy Dispersive Spectroscopy (EDS)[a] | | | | | |
|---|---|---|---|---|---|---|
| | Fe | C | O | S | Al | Si |
| Blank | + | + | – | – | + | + |
| B9 | + | – | + | – | + | – |
| B4 | + | + | + | + | + | + |

[a] Qualitative data: (+) and (–) symbols correspond to presence or absence of elements. The presence of Al and Si is attributed to a technical artifact and carrier contamination.

224 nm, Fig. 7d and f). The decrease in peak to peak height is also an indicator of alveolar corrosion, showing that all area analyzed was affected, producing a generalized corrosion. Although no formation of defects has been evidenced on the steel surface in contact with oil B9 (with TAN of 0.44 mg KOH $g^{-1}$), Fig. 7b, its topographic profile is noticeably altered, where the peak to peak height decreases practically by half (from 856 to 463 nm), Fig. 7e. Therefore, the corrosion process cannot be disregarded, existing in this case, in lower rate.

Similarly to AFM measurements, microphotographs of AISI 1020 steel from SEM analyzes were performed without and with exposure to crude oils B9 and B4, being shown in Fig. 8A–C, respectively. The presence of irregularities due to corrosion process is also confirmed from SEM measurements, Fig. 8B and C. The diameter of the eroded area is higher than its depth; therefore, the localized corrosion for AISI 1020 steel exposure to crude oils B9 and B4 is of the alveolar type [17]. The corrosion in AISI 1020 exposed to the B4 and B9, can be attributed due to TAN values, which the naphthenic corrosion takes place. This fact can be confirmed by the EDS measurements for both samples, where Fe and O are detected, Table 2. On the AISI 1020 exposed to crude oil B4, sulfur is also detected on the surface, in form of sulfur products [16]. Iron sulfide, for instance, can act as a passivation film may easily be cracked. In this case, since the EDS identify sulfur in AISI 1020 exposed to sample B4, sulfur corrosion and passivation process can be identified.

In general, the AISI 1020 steel corrosion process in the presence of naphthenic acid and sulfur compounds is described from Eqs. (1)–(3), where R denotes the naphthenic acid radical and $Fe(RCOO)_2$ is the corrosion product that is soluble in the oil medium (Eq. (1)). In presence of $H_2S$, a sulfide film is formed which can offer some protection depending on the acid concentration (Eqs. (2) and (3)) [7].

$$2RCOOH_{(soluble)} + Fe_{(solid)} \rightarrow Fe(RCOO)_{2(soluble)} + H_{2(g)} \quad (1)$$

$$H_2S_{(soluble)} + Fe_{(solid)} \rightarrow FeS_{(adsorbed)} + H_{2(g)} \quad (2)$$

$$Fe(RCOO)_{2(soluble)} + H_2S_{(soluble)} \rightarrow FeS_{(adsorbed)} + 2RCOOH_{(soluble)} \quad (3)$$

The absence of carbon in the EDS profile of AISI 1020 exposed to B9 crude oil is due the qualitative behavior of the technique in which the corrosion product can mask some elements. Also, the EDS is a technique of surface analysis. The presence of Al and Si in AISI 1020 exposed to sample B4 is attributed to the sandpapers used in the pretreatment of the steel, Table 2. Finally, the presence of oxygen/sulfur in the sample exposed to the acidic crude oil B4 indicates a more severe corrosivity, agreeing with SEM/EDS and AFM analyses.

## 4. Conclusion

Herein, we showed that the coupling of the two powerful analytical tools, negative-ion electrospray ionization Fourier transform ion cyclotron resonance mass spectrometry, ESI(-)FT-ICR MS, and atomic force microscopy (AFM) provided both chemical composition of naphthenic acids on molecular level ($C_cH_hN_nO_oS_s$) and the their corrosion power. As the petroleomics aims the correlation of molecular composition of crude oil with their physical and chemical characteristics and the impact of these characteristics in oil production, we illustraded the great potencial of AFM and ESI FT-ICR MS to predict the crude oil corrosion power.

The efficiency of naphthenic acids thermal decarboxylation was evaluated in a closed system in reflux at reduced pressure with heating temperature and time ranging from 280 to 350 °C and from 2 to 6 h, respectively. TAN results showed a reduction of 20% and 16% for crude oils A and B, being more efficient (reduction of 80%) at heating temperature of 350 °C during a period of 6 h (4.79 → 0.44 mg KOH $g^{-1}$).

From ESI(-)-FT-ICR MS data, the plots of DBE *versus* number carbon were constructed, being a useful tool for the understanding of extension of thermal degradation mechanism. Among aged oils samples, a reduction of amplitude of DBE values (from 1–15 to 1–12) is primarily observed in function of heating time (2 → 6 h). Finally, despite thermal decarboxylation process showed highly efficient and selective at 350 °C, compounds with DBE ranging from 1–15 and carbon number ranging from $C_{15}$ to $C_{45}$ still remains in crude oil after a period of 6 h of dercaboxylation.

AFM measurements evidenced the naphthenic acid corrosion *in situ* on AISI 1020 steel surface exposure to aged oil, with TAN of 4.73 mg KOH $g^{-1}$, providing a topographic profile profoundly altered by the peaks formation on the surface and a marked reduction in peak to peak height values (from 856 to 224 nm). Optical images and microphotographs confirmed the presence of irregularities, characterizing the corrosion mechanism as pitting type. The naphthenic corrosion was also evidenced in samples with low TAN value (0.44 mg KOH $g^{-1}$) from AFM results, cannot be ignored.

There are few studies so far that associate the corrosion profile obtained from AFM analysis with the molecular composition evaluated from ESI FT-ICR MS data. Therefore, it will be important development physico-chemical parameters based on AFM and FT-ICR data to evaluate the rate and type of corrosion. Herein, we believe that peak–peak height (parameter obtained by subtracting the value of the lowest peak by the highest peak in the specific topography area) will be able to monitor the extension of corrosion in function of exposure time; of steel (stainless or not); and of chemical composition of crude oils, and their fractions and cuts.

## Acknowledgments

This research was generously funded by PETROBRAS/CENPES, CNPq, and FINEP. GV, HPD, and PVD acknowledge FAPES and CAPES for fellowships. BGV acknowledges FAPEG for fellowship.

## Appendix A. Supplementary material

Supplementary data associated with this article can be found, in the online version, at http://dx.doi.org/10.1016/j.fuel.2014.02.031.

## References

[1] Moura LB, Guimarães RF, Abreu HFG, Miranda HC, Tavares SSM. Naphthenic corrosion resistance, mechanical properties and microstructure evolution of experimental Cr–Mo steels with high Mo content. Mater Res 2012;15(2):277–84.
[2] Barrow MP, Headley JV, Peru KM, Derrick PJ. Data visualization for the characterization of naphthenic acids within petroleum samples. Energy Fuels 2009;23:2592–9.
[3] Piehl R. Naphthenic acid corrosion in crude distillation units. Mater Perform 1988;27:37–43.
[4] Mapolelo MM, Rodgers RP, Blakney GT, Yen AT, Asomaning S, Marshall AG. Characterization of naphthenic acids in crude oils and naphthenates by

electrospray ionization FT-ICR mass spectrometry. Int J Mass Spectrom 2011;300:149–57.
[5] ASTM D664-09 Standard test Method for Acid Number of Petroleum Products by Potentiometric Titration.
[6] Shi Q, Zhao S, Xu Z, Chung KH, Zhang Y, Xu C. Distribution of acids and neutral nitrogen compounds in a chinese crude oil and its fractions: characterized by negative-ion electrospray ionization Fourier transform ion cyclotron resonance mass spectrometry. Energy Fuels 2010;24:4005–11.
[7] Slavcheva E, Shone B, Turnbull A. Review of naphthenic acid corrosion in oilrefining. Corros J 1999;34(2):125–31.
[8] Hsu CS, Dechert GJ, Robbins WK, Fukuda EK. Naphthenic acids in crude oils characterized by mass spectrometry. Energy Fuels 1999;14(1):217–23.
[9] Hsu CS, Hendrickson CL, Rodgers RP, McKenna AM, Marshall AG. Petroleomics: advanced molecular probe for petroleum heavy ends. J Mass Spectrom 2011;46:337–43.
[10] Gaspar A, Schrader W. Expanding the data depth for the analysis of complex crude oil samples by Fourier transform ion cyclotron resonance mass spectrometry using the spectral stitching method. Rapid Commun Mass Spectrom 2012;26:1047–52.
[11] McKenna AM, Purcell JM, Rodgers RP, Marshall AG. Heavy petroleum composition. 1. Exhaustive compositional analysis of athabasca bitumen HVGO distillates by Fourier transform ion cyclotron resonance mass spectrometry: A definitive test of the Boduszynski model. Energy Fuels 2010;24:2929–38.
[12] Fasciotti M, Lalli PM, Klitzke CF, Corilo YE, Pudenzi MA, Pereira RCL, et al. Petroleomics by traveling wave ion mobility-mass spectrometry using $CO_2$ as a drift gas. Energy Fuels 2013;27:7277–86.
[13] Klein GC, Angstrom A, Rodgers RP, Marshall AG. Use of saturates/aromatics/resins/asphaultenes (SARA) fractionation to determine matrix effects in crude oil analysis by electrospray ionization Fourier transform ion cyclotron resonance mass spectrometry. Energy Fuels 2006;20:668–72.
[14] Hsu CS, Hendrickson CL, Rodgers RP, McKenna AM, Marshall AG. Petroleomics: advanced molecular probe for petroleum heavy ends. J Mass Spectrom 2011;46(4):337–43.
[15] Savory JJ, Kaiser NK, McKenna AM, Xian F, Blakney GT, Rodgers RP, et al. Parts-per-billion Fourier transform ion cyclotron resonance mass measurement accuracy with a 'walking' calibration equation. Anal Chem 2011;83(5):1732–6.
[16] Cunico RL, Sheu EY, Mullins OC. Molecular weight measurement of UG8 asphaltene using APCI mass spectroscopy. Pet Sci Technol 2004;22(7–8):787–98.
[17] Purcell JM, Merdrignac I, Rodgers RP, Marshall AG, Gauthier T, Guibard I. Stepwise structural characterization of asphaltenes during deep hydroconversion processes determined by atmospheric pressure photoionization (APPI) Fourier transform ion cyclotron fesonance (FT-ICR) mass spectrometry. Energy Fuels 2010;24:2257–65.
[18] Benassi M, Berisha A, Romão W, Babayev E, Rompp A, Spengler B. Petroleum crude oil analysis using low-temperature plasma mass spectrometry. Rapid Commun Mass Spectrom 2013;27:825–34.
[19] Hughey CA, Rodgers RP, Marshall AG, Qian K, Robbins WK. Identification of acidic NSO compounds in crude oils of different geochemical origins by negative ion electrospray Fourier transform ion cyclotron resonance mass spectrometry. Organic Geochem 2002;33:743–59.
[20] Vaz BG, Abdelnur PV, Rocha WFC, Gomes AO, Pereira RCL. Predictive petroleomics: measurement of the total acid number by electrospray Fourier transform mass spectrometry and chemometric analysis. Energy Fuels 2013;27:1873–80.
[21] Huang BS, Yinb WF, Sang DH, Jianga ZY. Synergy effect of naphthenic acid corrosion and sulfur corrosion in crude oil distillation unit. Appl Surf Sci 2012;259:664–70.
[22] Freitas S, Malacarne MM, Romão W, Dalmaschio GP, Castro EVR, Celante VG, et al. Analysis of the heavy oil distillation cuts corrosion by electrospray ionization FT-ICR mass spectrometry, electrochemical impedance spectroscopy, and scanning electron microscopy. Fuel 2013;104:656–63.
[23] Dalmaschio GP, Malacarne MM, Almeida VMDL, Pereira TMC, Gomes AO, de Castro EVR, et al. Characterization of polar compounds in a true boiling point distillation system using electrospray ionization FT-ICR mass spectrometry. Fuel 2014;115:190–202.
[24] Piehl RL. Naphthenic acid corrosion in crude distillation units. Mater Perform 1988;27:37–43.
[25] Alvisi PP, Lins VFC. An overview of naphthenic acid corrosion in a vacuum distillation plant. Eng Fail Anal 2011;18:1403–6.
[26] Smith DF, Rodgers RP, Rahimi P, Teclemariam A, Marshall AG. Effect of thermal treatment on acidic organic species from athabasca bitumen heavy vacuum gas oil, analyzed by negative-ion electrospray Fourier transform ion cyclotron resonance (FT-ICR) mass spectrometry. Energy Fuels 2009;23:314–9.
[27] Mandal PC, Wahyudiono, Sasaki M, Goto M. Reduction of total acid number (TAN) of naphthenic acid (NA) using supercritical water for reducing corrosion problems of oil refineries. Fuel 2012;94:620–3.
[28] Ding L, Rahimi P, Hawkins R, Bhatt S, Shi Y. Naphthenic acid removal from heavy oils on alkaline earth-metal oxides and ZnO catalysts. Appl Catal A-Gen 2009;371:121–30.
[29] Colati KAP, Dalmaschio GP, de Castro EVR, Gomes AO, Vaz BG, Romão W. Monitoring the liquid/liquid extraction of naphthenic acids in brazilian crude oil using electrospray ionization FT-ICR mass spectrometry (ESI FT-ICR MS). Fuel 2013;108:647–55.
[30] ASTM D4294-10 Standard Test Method for Sulfur in Petroleum and Petroleum Products by Energy Dispersive X-ray Fluorescence Spectrometry; 2000.
[31] ASTM D 2892. Standard Test Method for Distillation of Crude Oil; 2005.
[32] Pereira TMC, Vanini G, Oliveira ECS, Cardoso FMR, Fleming FP, Neto AC, et al. An evaluation of the aromaticity of asphatenes using atmospheric pressure photoionization Fourier transform ion cyclotron resonance mass spectrometry – APPI(±)FT-ICR MS. Fuel 2001;117:348–457.
[33] Binnig G, Quate CF, Gerber CH. Atomic force microscopy. Phys Rev Lett 1986;56:930–3.
[34] Batina N, Manzano-Martinez JC, Andersen SI, Lira-Galeana C. AFM characterization of organic deposits on metal substrates from mexican crude oils. Energy Fuels 2003;17:532–42.
[35] Nakai Y, Fujiwarw S, Ogawa T, Shimizu Y. Observations of corrosion fatigue crack initiation processes in metals by means of AFM. Mater Sci Res Int, Special Techn Publication 2001;1:101–6.
[36] Dufrêne, Yves F. AFM for nanoscale microbe analysis. Analyst 2008;133:297–301.
[37] Zhang A, Ma Q, Wang K, Liu X, Shuler P, Tang Y. Naphthenic acid removal from crude oil through catalytic decarboxylation on magnesium oxide. Appl Catal A-Gen 2006;303:103–9.
[38] Blum SC, Olmstead WN, Bearden R Jr. Thermal decomposition of naphthenic acids. U.S. Patent 1996; 5:750.
[39] Hughey CA, Rodgers RP, Marshall AG. Resolution of 11,000 compositionally distinct components in a single electrospray ionization Fourier transform ion cyclotron resonance mass spectrum of crude oil. Anal Chem 2002;74:4145–9.
[40] Hughey CA, Hendrickson CL, Rodgers RP, Marshall AG. Kendrick mass defect spectroscopy: a compact visual analysis for ultrahigh-resolution broadband mass spectra. Anal Chem 2001;73:4676–81.
[41] Van Krevelen DW. Graphical-statistical method for the study of structure and reaction processes of coal. Fuel 1950;29:269–84.
[42] Schaub TM, Jennings DW, Kim S, Rodgers RP, Marshall AG. Heat-exchanger deposits in an inverted steam-assisted gravity drainage operation. Part 2. organic acid analysis by electrospray ionization Fourier transform ion cyclotron resonance mass spectrometry. Energy Fuels 2007;21:185–94.
[43] BaiBing Y, ChunMing X, SuoQi Z, Samuel HC, Keng HC, Quan S. Thermal transformation of acid compounds in high TAN crude oil. Sci China Chem 2013;56:848–55.